

Stable suspension and dispersion-induced transitions from repulsive Casimir forces between fluid-separated eccentric cylinders

Alejandro W. Rodriguez,¹ J. N. Munday,² J. D. Joannopoulos,¹ Federico Capasso,² Diego A. R. Dalvit,³ and Steven G. Johnson⁴

¹*Department of Physics, Massachusetts Institute of Technology, Cambridge, MA 02139*

²*Department of Applied Physics, Harvard University, MA 02139*

³*Theoretical Division, Los Alamos National Laboratory, Los Alamos, NM 87545*

⁴*Department of Mathematics, Massachusetts Institute of Technology, Cambridge, MA 02139*

Using exact numerical methods for finite-size nonplanar objects, we demonstrate a stable mechanical suspension of a silica cylinder within a metallic cylinder separated by ethanol, via a repulsive Casimir force between the silica and the metal. We investigate cylinders with both circular and square cross sections, and show that the latter exhibit a stable orientation as well as a stable position, via a method to compute Casimir torques for finite objects. Furthermore, the stable orientation of the square cylinder is shown to undergo an unusual 45° transition as a function of the separation length-scale, which is explained as a consequence of material dispersion.

The Casimir force, arising from quantum fluctuations of the electromagnetic field, was first described as an attractive, monotonically decaying force between metallic plates [1]. It can become repulsive in special circumstances, e.g. involving fluid-separated asymmetric plates [2]. It has been proposed that repulsive Casimir forces between fluid-separated objects can lead to stable mechanical equilibria, and hence frictionless static bearings or other interesting passive-suspension devices [3, 4, 5]. However, previous calculations and experiments involving fluid-separated objects have been restricted to geometries involving parallel plates or approximations thereof [6] (similar to experiments involving air-separated metals [4, 7]). Here, using recently developed numerical techniques [8, 9], we present accurate theoretical calculations of Casimir forces between fluid-separated objects with finite square and circular cross sections (Fig. 1 insets) that rigorously demonstrate stable Casimir equilibria [25]. (A similar geometry involving vacuum-separated perfectly-metallic circular cylinders has been solved analytically and shown to exhibit an unstable equilibrium [10].) In the case of square cross sections, we also obtain the stable orientational equilibrium with respect to rotations. We present a numerical method to accurately compute the Casimir torque on a finite object (in contrast to previous heuristics [11] or analytical results for semi-infinite planes (half-spaces) [3, 12, 13]), and obtain a surprising result—the stable orientation changes by 45° depending on the length-scale, a feature that we show to be a consequence of material dispersion. For certain fluid-separated materials, the frequency dependence of the permittivity (material dispersion) causes the Casimir force to switch from repulsive to attractive at some critical separation [2]; this leads to the orientation transition described here, and may produce other length-scale-based qualitative transitions in future geometries.

A repulsive Casimir force arises between parallel plates of permittivity ϵ_1 and ϵ_2 separated by a fluid of permittivity ϵ_f , if $\epsilon_1(i\xi) < \epsilon_f(i\xi) < \epsilon_2(i\xi)$ for a sufficiently wide range of imaginary frequencies $\xi = \text{Im } \omega$ [2]. Three such materials are silica (SiO_2) and metal (Au) separated by ethanol [4], discussed in more detail below. We investigated the three-

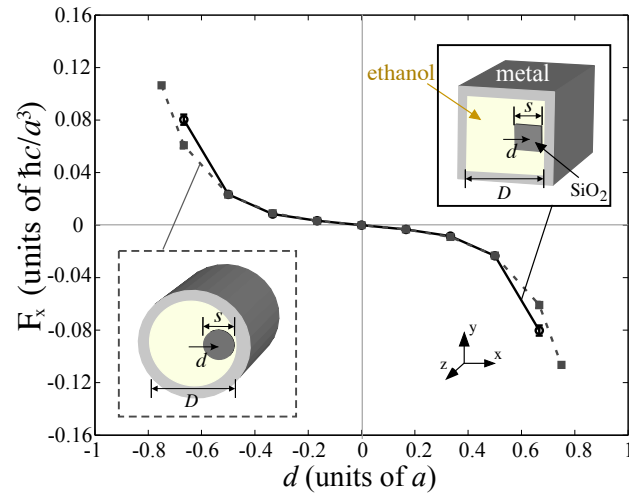


FIG. 1: Casimir force F_x in the x -direction, per unit z -length, on a silica cylinder suspended within a perfectly-metallic cylinder (inset), separated by fluid (ethanol), as a function of the x -displacement from equilibrium (eccentricity) d [in units of $a = 0.5(D - s)$] for both circular (solid-line) and square (dashed-line) cylinders. $d = 0$ is seen to be a stable equilibrium.

dimensional (constant cross-section) geometries shown in the inset of Fig. 1: square or circular SiO_2 cylinders of diameter s surrounded by a metal cylinder of diameter D , separated by ethanol. For computational convenience, we use a perfect metal [$\epsilon(i\xi) \rightarrow \infty$, corresponding to negligible skin depth] for the outer cylinder, but we use experimental ω -dependent permittivities for the SiO_2 and ethanol. The resulting plot in Fig. 1, computed as described below, shows the force per unit z -length on the inner cylinder as a function of the displacement from equilibrium d (eccentricity, or center-to-center cylinder separation) in units of a , where $a \equiv 0.5(D - s) = 0.0955 \mu\text{m}$ so that $d/a = \pm 1$ for touching surfaces, for parameters $s/D = 0.25$. Figure 1 demonstrates a stable equilibrium with respect to displacements from $d = 0$ for both square (solid black) and circular (dashed grey) cross sections.

In such geometries, with bodies of sizes and curva-

tures comparable to their separations, approximations of the Casimir force as a pairwise attraction between surfaces are not valid and may yield qualitative errors [9, 14, 15]. Instead, we employ a computational method introduced in Ref. 8, based on integration of the mean electromagnetic stress tensor evaluated in terms of the imaginary-frequency Green's function via the fluctuation-dissipation theorem [8]. (Although the classical stress tensor at real frequencies is problematic to evaluate within dispersive media such as the fluid here, the imaginary-frequency mean stress tensor of the Casimir force is still valid in this case [16].) The computation involves repeated evaluation of the electromagnetic Green's function, integrated over imaginary frequency $i\xi$ and a surface around the object of interest. The Green's function is the inverse of the linear operator $[\nabla \times \nabla \times + \xi^2 \varepsilon(i\xi, \mathbf{r})]$, which here is discretized using a finite-difference Yee grid, and inverted using the conjugate-gradient method [8]. The experimental permittivities of SiO_2 and ethanol were fit to a standard multiple-oscillator model [17] that is accurate over a wide range of infrared to ultraviolet wavelengths: $\varepsilon(i\xi) = 1 + \sum_{n=1}^N C_n [1 + (\xi/\omega_n)^2]^{-1}$, in terms of parameters ω_n and C_n fit to experiments. The parameters we used are [18, 19]: ethanol ($N = 2$) $\omega_n = \{6.6, 114\} \times 10^{14}$ Hz and $C_n = \{23.84, 0.852\}$; SiO_2 ($N = 3$) $\omega_n = \{0.867, 1.508, 203.4\} \times 10^{14}$ Hz and $C_n = \{0.829, 0.095, 1.098\}$. The Casimir force \mathbf{F} is computed as an integral of the form $\mathbf{F} \sim \int_0^\infty d\xi \iint \langle \mathbf{T} \rangle d\mathbf{A}$ [8], where the mean stress tensor $\langle \mathbf{T} \rangle$ is computed at each position and frequency from the Green's function as described above. Below, we also analyze the Casimir torque $\boldsymbol{\tau}$, which can be computed in the same framework, with a minor modification, $\boldsymbol{\tau} \sim \int_0^\infty d\xi \iint \mathbf{r} \times (\langle \mathbf{T} \rangle d\mathbf{A})$, as proposed in our earlier work [8].

In order to obtain a simpler understanding of the various features in Fig. 1, as well as to clarify some of the subsequent results, we now turn to an analogous one-dimensional geometry, depicted on the inset of Fig. 2: a SiO_2 slab of thickness s , separated from two metallic half-spaces, a (surface-to-surface) distance $a \equiv 0.5(D - s)$ from the SiO_2 surface, with ethanol (fluid) in between. This geometry can be easily analyzed precisely by a generalization of the Lifshitz formula that expresses the Casimir force in terms of an integral based on reflection coefficients of the multilayer structure [20]. Figure 2 shows the force per unit area on the inner slab (again using $s/D = 0.25$), as a function of the displacement d as before, for two length-scales: $a = 0.0955 \mu\text{m}$ (red), and $a = 0.6 \mu\text{m}$ (black). Three interesting features can be observed. First, there is a stable equilibrium at $d = 0$, just as for the two-dimensional stable equilibrium in Fig. 1. Second, in the case of the perfectly-metallic half-spaces, the force changes sign at a critical distance d_c that depends on the length-scale a . Third, if we assume the metallic half-spaces to be made out of the real metal gold (Au), shown by the dashed line for $a = 0.0955 \mu\text{m}$, this transition disappears, and the force is always repulsive. (We model the dielectric constant of Au by the usual Drude model $\varepsilon(i\xi) = 1 + \omega_p^2/\xi(\xi + \gamma)$,

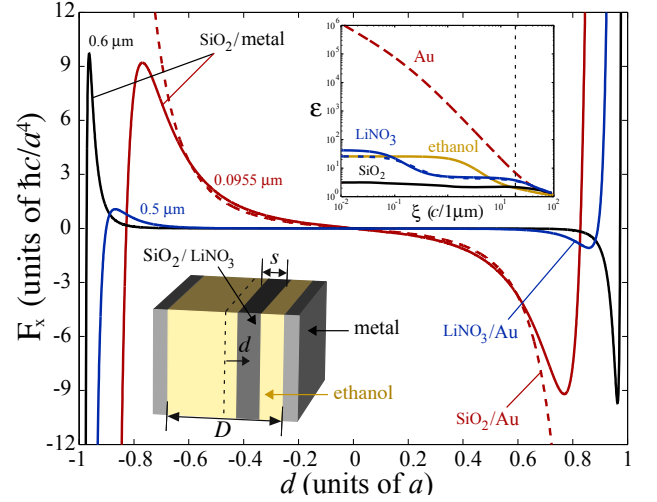


FIG. 2: Casimir force F_x in the x -direction, per unit area, between a planar silica slab suspended between two perfect-metal plates (solid red and black lines) or gold half-spaces (dashed red line), separated by a fluid (ethanol), as a function of the dimensionless x -displacement d from equilibrium. The force is plotted also at two length-scales $a \equiv 0.5(D - s) = 0.0955 \mu\text{m}$ (red lines) and $a = 0.6 \mu\text{m}$ (black line). The solid blue line shows the same quantity for the case of a lithium-niobate slab and a gold half-space, for $a = 0.5 \mu\text{m}$. (Insets:) Top inset: $\varepsilon(i\xi)$ for SiO_2 (black), LiNbO_3 (solid and dashed blue), ethanol (orange) and Au (red) as a function of imaginary frequency ξ . Bottom inset: schematic of geometry.

where $\omega_p = 1.367 \times 10^{14}$ Hz and $\gamma = 5.320 \times 10^{13}$ Hz [19]). To explain these features, we refer to the inset of Fig. 2, which shows the dielectric properties of the SiO_2 , ethanol and Au (in dimensionless frequency units of $c/1 \mu\text{m}$). The key point is that the contributions to the Casimir force come primarily from imaginary “wavelengths” $2\pi/\xi$ larger than some length-scale set by the separation, while very short wavelengths (large ξ) on this scale are exponentially cut off in the force integral [21]. So, for large length-scales a , the force is dominated by the small- ξ permittivities, which are in the correct order $\varepsilon_{\text{silica}} < \varepsilon_{\text{ethanol}} < \varepsilon_{\text{metal}}$ to obtain a repulsive force and a stable equilibrium. On the other hand, for small length-scales and separations, large- ξ contributions become more and more important, and at large ξ the ordering switches to $\varepsilon_{\text{silica}} > \varepsilon_{\text{ethanol}}$ (for $\xi > 2.3 c/\mu\text{m}$, where the intersection point is marked by the vertical dashed line on the inset of Fig. 2), leading to attractive contributions to the force. For the case of the perfect metal, these attractive contributions are large enough to flip the sign of the total force for small separations, whereas for Au the attractive high- ξ contributions are suppressed by the diminishing $\varepsilon(i\xi)$ of the Au (as the three permittivities become equal, their force contribution vanishes) and the force remains repulsive. As discussed below, this repulsive-attractive transition produces an interesting effect on the stable orientation in the case of nested squares. While the latter is absent in the SiO_2 -ethanol-Au configuration, we have calculated the force between ethanol-separated lithium-niobate LiNbO_3 and Au plates and found

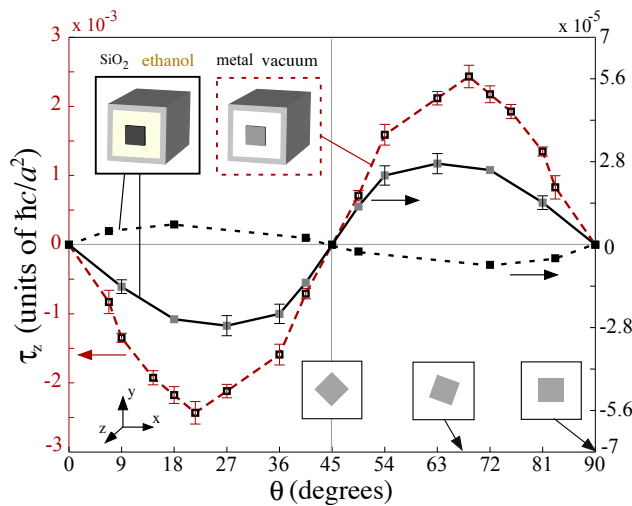


FIG. 3: Casimir torque τ_z , per unit z -length, on the inner square rod of eccentric square cylinders as a function of the angle θ with respect to the x -axis (see right insets) for two square cylindrical geometries depicted on the top insets (see text). Error bars are estimates of the effect of finite grid resolution.

a sign transition at separations $\sim 0.05 \mu\text{m}$. This is illustrated in Fig. 2 (solid blue line); because LiNbO_3 's anisotropy greatly complicates the modeling, we used a PFA approximation based on summing the Lifshitz forces between semi-infinite Au and LiNbO_3 slabs (neglecting the finite LiNbO_3 thickness). The two principal values of the permittivity tensor of LiNbO_3 [19] are plotted in the inset. There are also transitions for ethanol-separated barium-titanate and calcite plates at separations $\sim 0.01 \mu\text{m}$ [3]. Since the LiNbO_3 -ethanol-Au and barium-ethanol-calcite cases are much more difficult to compute (the outer cylinder is not a perfect metal and LiNbO_3 is anisotropic), we focus on the SiO_2 -ethanol-metal case here, which exhibits similar qualitative behaviors.

The square cylinder geometry must, from symmetry considerations, have two equilibrium orientations ($\theta = 0^\circ$ and $\theta = 45^\circ$). *A priori*, it is not clear which of the two configurations is stable, and under what circumstances. To answer these questions, Fig. 3 plots the Casimir torque per unit z -length on the inner square, as a function of the angle of rotation θ between the inner and outer squares (depicted graphically by the insets). In addition to computing the torque for the stable equilibrium structure consisting of SiO_2 -ethanol-perfect-metal (repulsive forces), we also analyze the torque on an inner cylinder when both cylinders are perfectly metallic and separated by vacuum, in which case the forces are purely attractive and there is no stable equilibrium with respect to displacements.

The resulting torque per unit z -length is shown in Fig. 3, for both the repulsive (solid, filled-square-lines) and attractive (solid, open-square-line) cases, as θ is varied from 0° to 90° (all other angles are redundant by symmetry)—by the repulsive case, we mean the SiO_2 -ethanol-Au suspended structure of Fig. 1. The stable torque configuration for both repulsive

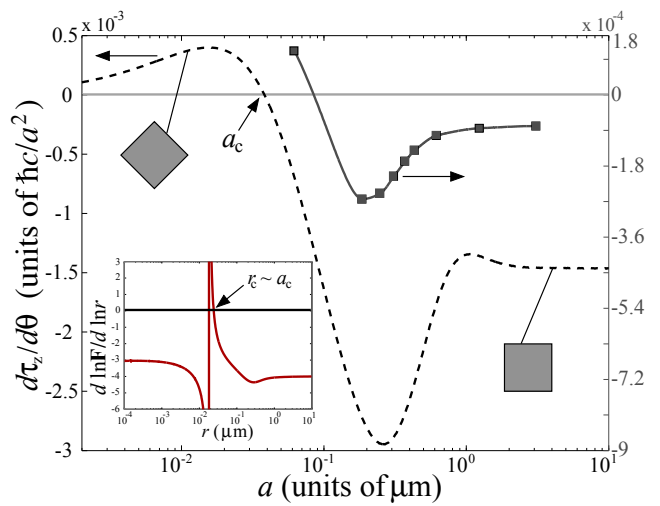


FIG. 4: Derivative of the Casimir torque in the z -direction with respect to θ , $d\tau_z/d\theta$, in units of $\hbar c/a^2$, evaluated at $\theta \approx 0$, as a function of length-scale $a = 0.5(D - s)$. The solid line is a shape-preserving fit to the exact Casimir torque as computed by our numerical method (solid squares), and the dashed line is the same quantity as computed by a PFA approximation. Both curves display a change (dispersion-induced transition) in the stable orientation of the square. (*Inset:*) Slope of the force between SiO_2 and metallic half-spaces (ethanol-separated) $d \ln F/d \ln r$ as a function of separation r , in units of μm .

and attractive cases corresponds to the $\theta = 45^\circ$ orientation, a surprising result considering the difference in the sign of the force. A stable orientation of 45° in the purely metallic case is not surprising, since an attractive force that decreases with separation should intuitively (in the heuristic picture of pairwise attractions between surfaces) favor an orientation where the surfaces are as close as possible (with the closest-surface interactions dominating), hence pulling the corners of the inner square towards the outer surfaces. On the other hand, a repulsive force should intuitively push the surfaces as far apart as possible, which would seem to suggest a 0° stable orientation for the repulsive case. The reason for this apparent contradiction between intuition and the numerical results of Fig. 3 lies in the effects of material dispersion. In particular, if we neglect the frequency dispersion of SiO_2 and ethanol, and use only the $\xi \rightarrow 0$ dielectric constants, the torque as a function of θ (shown as the dashed black line in Fig. 3) indeed exhibits a stable orientation at $\theta = 0^\circ$, as expected from the simple pairwise intuition: in this case, the force between SiO_2 and perfect metal separated by ethanol is repulsive at *all* length-scales, since dispersion is absent, and decays as $1/r^4$ as for perfect metals.

The above results indicate the existence of a “critical” length-scale a_c at which the orientation of the cylinder changes by 45° . One way to determine a_c is to calculate the derivative of the torque on the inner cylinder at $\theta = 45^\circ$ as a function of a , and to look for a change in the sign when $a = a_c$. This derivative is plotted as the solid line in Fig. 4, with the derivative computed by a center-difference approximation,

and exhibits the expected transition from stable [$d\tau_z/d\theta > 0$, Fig. 4 (left-square inset)] to unstable [$d\tau_z/d\theta < 0$, Fig. 4 (right-square inset)] at $a_c \approx 0.1 \mu\text{m}$, a consequence of material dispersion. A better understanding of this transition can be gained by inspecting a simple pairwise surface-surface interaction heuristic, the proximity-force approximation (PFA). PFA is only an *ad hoc* model, in which the force on each point of the surface (and hence the torque) is treated as simply the “parallel-plate” force between fluid-separated half-spaces (with “lines of interaction perpendicular” to the outer surface). This simple model captures the qualitative features of the transition in the stable orientation, as shown by the dashed line in Fig. 4, although it is of course quantitatively incorrect (overestimating the torque [13] by nearly an order of magnitude). The insight that one gains from the PFA model, however, is a relation between the point a_c and the pairwise force law. The transition a_c does *not* occur at the a where the force switches from repulsive to attractive. Rather, it occurs when the *slope* $d \ln F / d \ln r$ with separation r (Fig. 4 inset) becomes zero—that is, when the force is no longer growing as the separation decreases, even if the force remains repulsive, it is no longer advantageous to bring the surface closer.

We are hopeful that the phenomena described in this paper will be amenable to experiment, since despite this nonplanar geometry, they circumvent two important challenges common to other Casimir experiments. First, the difficulty of achieving concentric surfaces is greatly reduced by the fact that the parallel configuration is a stable equilibrium, in contrast to the instability of parallel attractive plates. Second, the difficulty of eliminating static-charge effects is ameliorated by the fact that electrostatic effects cannot produce a stable equilibrium in this geometry, and the fields of any static charge on the outer conducting cylinder will be shielded from the inner cylinder [10]. (If we inverted the geometry, so that the silica was on the outside and the metal was on the inside, then the fact that the static permittivity of the fluid is larger than that of the silica would lead to a classical stable equilibrium for a charged metal inner cylinder [22, 23]; this does not contradict Earnshaw’s theorem because the forces are due to induced charges [24].) Obviously, an experiment cannot employ a perfectly conducting outer cylinder like the one in our calculations. Nevertheless, we expect that a similar stable equilibrium will be obtained for real metals, as in our one-dimensional calculation with Au in Fig. 2. Finally, as noted above, there are a number of materials that exhibit a transition from repulsive to attractive interactions (unlike the SiO_2 –ethanol–Au combination), and they should therefore display the orientational transition.

This work was supported in part by U. S. Department of Energy Grant No. DE–FG02–97ER25308, the NSF MRSEC program under Grant No. DMR–0213282, and by the MIT

Ferry Fund.

-
- [1] H. B. G. Casimir, Proc. K. Ned. Akad. Wet. **51**, 793 (1948).
 - [2] I. E. Dzyaloshinskii, E. M. Lifshitz, and L. P. Pitaevskii, Adv. Phys. **10**, 165 (1961).
 - [3] J. N. Munday, D. Iannuzzi, Y. Barash, and F. Capasso, Phys. Rev. A **71**, 042102 (2005).
 - [4] F. Capasso, J. N. Munday, D. Iannuzzi, and H. B. Chan, IEEE J. Selected Topics in Quant. Elec. **13**, 400 (2007).
 - [5] D. Iannuzzi, J. Munday, and F. Capasso, US Patent Application US20070066494 (2006).
 - [6] J. N. Munday and F. Capasso, Phys. Rev. A **75**, 060102(R) (2007).
 - [7] S. K. Lamoreaux, Phys. Rev. Lett. **78**, 5 (1997). U. Mohideen and A. Roy, Phys. Rev. Lett. **81**, 4549 (1998). H. B. Chan, V. A. Aksyuk, R. N. Kleinman, D. J. Bishop, and F. Capasso, Science **291**, 1941 (2001). R. S. Decca, D. Lopez, E. Fischbach, and D. E. Krause, Phys. Rev. Lett. **91**, 050402 (2003).
 - [8] A. Rodriguez, M. Ibannescu, D. Iannuzzi, J. D. Joannopoulos, and S. G. Johnson, Phys. Rev. A **76**, 032106 (2007).
 - [9] A. Rodriguez, M. Ibannescu, D. Iannuzzi, F. Capasso, J. D. Joannopoulos, and S. G. Johnson, Phys. Rev. Lett. **99**, 080401 (2007).
 - [10] D. A. R. Dalvit, F. C. Lombardo, F. D. Mazzitelli, and R. Onofrio, Phys. Rev. A **74**, 020101 (2006).
 - [11] A. Scardicchio and R. L. Jaffe, Nuclear Physics B. **704**, 552 (2005).
 - [12] S. J. van Enk, Phys. Rev. A **52**, 2569 (1995). C.-G. Shao, A.-H. Tong, and J. Luo, Phys. Rev. A **72**, 022102 (2005). H. Razmi and S. M. Modarresi, Int. J. Theor. Phys. **44**, 229 (2005).
 - [13] R. B. Rodrigues, P. A. Maia Neto, A. Lambrecht, and S. Reynaud, Europhys. Lett. **75**, 822 (2006).
 - [14] D. A. R. Dalvit, F. C. Lombardo, F. D. Mazzitelli, and R. Onofrio, Europhys. Lett. **67**, 517 (2004).
 - [15] H. Gies and K. Klingmuller, Phys. Rev. Lett. **96**, 220401 (2006).
 - [16] L. P. Pitaevskii, Phys. Rev. A **73**, 047801 (2006).
 - [17] J. Mahanty and B. W. Ninham, *Dispersion forces* (Academic London, 1976).
 - [18] A. Milling, P. Mulvaney, and I. Larson, J. Colloid and Interface Science **180**, 460 (1996).
 - [19] L. Bergstrom, Adv. Colloid and Interface Science **70**, 125 (1997).
 - [20] M. S. Tomaš, Phys. Rev. A **66**, 052103 (2002).
 - [21] E. M. Lifshitz, Sov. Phys. JETP **2**, 73 (1956).
 - [22] R. Y. Chiao and J. Boyce, Phys. Rev. Lett. **73**, 3383 (1994).
 - [23] D. A. R. Dalvit, F. C. Lombardo, F. D. Mazzitelli, and R. Onofrio, Europhys. Lett. **65**, 517 (2004).
 - [24] P. W. Milonni, D. F. V. James, and H. Fearn, Phys. Rev. Lett. **75**, 3194 (1995).
 - [25] Here, we focus strictly on Casimir forces and ignore external forces such as gravity. We consider only static situations, so viscous forces are not present, nor is surface tension important for rigid immersed objects.